

Indirect and direct detection prospect for TeV dark matter in the MSSM-9

Maria Eugenia Cabrera-Catalan

Instituto de Física, Universidade de São Paulo, C.P. 66.318, 05315-970 São Paulo, Brazil
Instituto de Física Teórica, IFT-UAM/CSIC, U.A.M. Cantoblanco, 28049 Madrid, Spain and
GRAPPA Institute, University of Amsterdam, 1098 XH Amsterdam, The Netherlands

Shin'ichiro Ando, Christoph Weniger, and Fabio Zandanel

GRAPPA Institute, University of Amsterdam, 1098 XH Amsterdam, The Netherlands

(Dated: October 13, 2018)

We investigate the prospects of indirect and direct dark matter searches within the minimal supersymmetric standard model with nine parameters (MSSM-9). These nine parameters include three gaugino masses, Higgs, slepton and squark masses, all treated independently. We perform a Bayesian Monte Carlo scan of the parameter space taking into consideration all available particle physics constraints such as the Higgs mass of 126 GeV, upper limits on the scattering cross-section from direct-detection experiments, and assuming that the MSSM-9 provides all the dark matter abundance through thermal freeze-out mechanism. Within this framework we find two most probable regions for dark matter: 1-TeV higgsino-like and 3-TeV wino-like neutralinos. We discuss prospects for future indirect (in particular the Cherenkov Telescope Array, CTA) and direct detection experiments. We find that for slightly contracted dark matter profiles in our Galaxy, which can be caused by the effects of baryonic infall in the Galactic center, CTA will be able to probe a large fraction of the remaining allowed region in synergy with future direct detection experiments like XENON-1T.

I. INTRODUCTION

Identifying the particle nature of dark matter is one of the most pressing goals of modern astrophysics and cosmology. If dark matter is made of weakly interacting massive particles (WIMPs) [1, 2], where the relic dark matter abundance is naturally explained with the thermal freeze-out mechanism, a particular promising avenue is the search for signatures from the self-annihilation of dark matter particles in gamma rays [3]. The required average velocity-weighted annihilation cross-section during freeze-out is of the order of $\langle\sigma v\rangle = 3 \times 10^{-26} \text{ cm}^3 \text{ s}^{-1}$ [1, 4]. Upper limits from modern gamma-ray instruments, such as the Large Area Telescope (LAT) aboard *Fermi* satellite, start to exclude this canonical annihilation cross-section for WIMP masses below 100 GeV [5]. At the same time, the hunt for signatures of physics beyond the standard model of particle physics, especially of supersymmetry, is ongoing at the Large Hadron Collider (LHC). Supersymmetric models provide interesting candidate particles for WIMP dark matter (in most cases the lightest neutralino). Although there has been no claim of positive signatures of supersymmetry yet, some outstanding conclusions can be drawn from several measurements at the LHC. One of them comes from the mass measurement of the Higgs boson of about 126 GeV [6, 7].

Since particle masses and couplings are subject to loop corrections, the Higgs mass measurement can provide indirect information about yet undiscovered particles. Therefore, this measurement already significantly constrains the parameter space of supersymmetric models. Reference [8] studied the implications of the Higgs mass measurement for the minimal supersymmetric standard model (MSSM) with five parameters (the con-

strained MSSM), and found that the posterior probabilities for these parameters are narrowly distributed. Reference [9] further extended the model to include the non-universality in gaugino and Higgs masses, and found qualitatively similar results. The most probable masses of neutralino dark matter were found to be around 1 TeV, for higgsino dark matter, and 3 TeV, for wino dark matter.

The wino dark matter case is already in some tension with searches for gamma-ray lines [10–12]. The wino dark matter annihilation cross-section is significantly larger than the canonical value for WIMPs due to a non-perturbative effect known as Sommerfeld Enhancement (SE) [13–17]. The SE calculation for heavy WIMPs is subject to large logarithmic corrections due to the large hierarchy between the dark matter mass and the W -boson mass. Reference [18] showed that full one-loop computation makes the cross-section smaller up to about 30% with respect to the SE correction at tree level. Even more precise computations using Soft Collinear Effective Theory were recently presented [19–22]. Reference [22] found that when calculating leading-log semi-inclusive rates, the effect of higher order corrections are very modest.

There are several studies in the literature that have incorporated the impact of the Higgs mass measurement, and of XENON-100 [23] and LUX [24] bounds, on the WIMP-nucleon spin-independent scattering cross-section on constrained MSSM scenarios (see, e.g., Refs. [8, 9, 25–30]). Various statistical approaches have been used to infer the most probable regions of these scenarios. The parameter space is often restricted to energies below a few TeV, according to what is expected from “natural” supersymmetry. Interestingly, when performing a proper

Bayesian analysis, the fine-tuning penalization arises automatically from very basic statistical arguments (the Bayesian version of “Occam’s razor”), allowing to explore larger regions of the parameter space while taking the notion of naturalness automatically into account (see, e.g., Ref. [31]).

Reference [9] studied the non-universal higgsino and gaugino masses model within the Bayesian framework. The authors showed that the most probable regions for the neutralino dark matter are around 1 TeV (higgsino dark matter) and 3 TeV (wino dark matter), the high masses being mostly due to the Higgs mass and the relic density constraint. Although this leaves a very large portion of the favoured supersymmetric parameter space outside the reach of LHC, prospects for future dark matter experiments were shown to be very promising, in particular for XENON-1T [32] for direct detection, and for the Cherenkov Telescope Array (CTA) [33] for indirect searches. Recently, Ref. [34] presented a first study of the detection prospects for CTA and XENON-1T for neutralino dark matter in the 19-parameter phenomenological MSSM. In this study, the SE was effectively included as an extrapolation of the results from Refs. [15, 17].

In the present paper, we study consequences of MSSM models with extended nine parameters (MSSM-9), and prospects for indirect and direct dark matter searches. In addition to the non-universality of the gaugino and Higgs masses studied in Ref. [9], we investigate the non-universality of masses and the trilinear couplings in the sfermion sector (i.e., they are independent between sleptons and squarks). This treatment is more general because constraints from the LHC mainly affect the squark and gluino sector and do not directly reflect on the sleptons. Since the preferred dark matter masses are at 1 TeV and above, we discuss constraints from the *Fermi* gamma-ray satellite and current generation of Cherenkov telescopes, in particular HESS [35]. As mentioned above, the wino dark matter around 3 TeV is subject to the SE correction of the annihilation cross-section [14, 17, 18, 36], and, therefore, we calculate the SE point-by-point in the scan. In addition, the annihilation of wino dark matter also yields strong gamma-ray line signals, which are tightly constrained by the HESS observations of the Galactic center [35]. Note that our results are based on a full numerical study of MSSM parameter scan, and does not rely on a simplifying assumption of *pure* wino case as adopted in Refs. [10–12]. We will discuss prospects for future indirect and direct detection experiments, most notably for CTA that will have an excellent sensitivity for gamma rays above 100 GeV [37–41].

The paper is organized as follows. In section II, we discuss the model and the adopted scanning technique. We will summarize the results of the scan in section III, and show in section IV prospects for future indirect and direct detection experiments. In section V, we give our conclusions.

II. MSSM MODELS AND HIGGS MASS

The discovery of the Higgs boson [6, 7] has completed the picture of the standard model of particle physics, which has proven an extremely good description of particle physics up to the TeV scale. Beyond the crucial importance of this discovery by itself, this result has far-reaching consequences for well-motivated candidates of physics beyond the standard model, such as supersymmetry, and in particular for the MSSM.

The rather high reported Higgs mass m_h shifts the scale of supersymmetry to higher values. In the MSSM, the tree-level Higgs mass is bounded by the mass of the Z -boson, and, therefore, large radiative corrections are needed in order to reconcile theory and experiment. An approximate analytic formula for m_h [42, 43] reads

$$m_h^2 \simeq M_Z^2 \cos^2 2\beta + \frac{3}{4\pi^2} \frac{m_t^4}{v^2} \left[\log \frac{M_{\text{SUSY}}^2}{m_t^2} + \frac{X_t^2}{M_{\text{SUSY}}^2} \left(1 - \frac{X_t^2}{12M_{\text{SUSY}}^2} \right) \right] + \dots, \quad (1)$$

where $\tan \beta$ is the ratio between the vacuum expectation values of the two Higgs doublets $v_u = \langle H_u^0 \rangle$ and $v_d = \langle H_d^0 \rangle$, $v^2 = v_u^2 + v_d^2$, m_t is the top running mass, and M_{SUSY} represents a certain average of stop masses. $X_t = A_t - \mu \cot \beta$, where μ is the Higgs mass term in the superpotential, and A_t is the trilinear stop coupling, both at the electroweak breaking scale. The first term of Eq. (1) is the tree-level Higgs mass, while the second two terms are the dominant radiative and threshold corrections. Note that the radiative corrections grow logarithmically with the stop masses while the threshold corrections has a maximum for $X_t = \pm\sqrt{6}M_{\text{SUSY}}$. To achieve $m_h \simeq 126$ GeV, one typically needs stop masses larger than ~ 3 TeV, unless X_t is close to its maximum value.

In order to evaluate the sensitivity on dark matter in a more generic context, we parameterize the MSSM with 10 fundamental parameters at the gauge coupling unification scale. After requiring the correct electroweak symmetry breaking, we end up with 9 effective parameters:

$$\left\{ s, M_1, M_2, M_3, m_{\tilde{q}}, m_{\tilde{l}}, m_H, A_0^{\tilde{q}}, A_0^{\tilde{l}}, \tan \beta, \text{sgn}(\mu) \right\} \quad (2)$$

where s represents the SM nuisance parameters, M_1, M_2, M_3 are the gaugino masses, $m_{\tilde{q}}, m_{\tilde{l}}$ are the squark, slepton, and Higgs masses ($m_H = m_{H_u} = m_{H_d}$), and $A_0^{\tilde{q}}$ and $A_0^{\tilde{l}}$ are the squark and slepton trilinear couplings. The sign of μ is fixed to +1. All the soft parameters defined at gauge coupling unification scale, except for $\tan \beta$ and the SM nuisance parameters. Compared with Ref. [9], we further generalize the sfermion sector, by adopting independent values for squarks and sleptons.

We perform a Bayesian analysis to generate a map of the relative probability of different regions of the parameter space. In doing so, the global likelihood is defined as

Observable	Mean value	Uncertainties		Ref.
	μ	σ (exper.)	τ (theor.)	
M_W [GeV]	80.399	0.023	0.015	[44]
$\sin^2 \theta_{eff}$	0.23153	0.00016	0.00015	[44]
$\text{BR}(\bar{B} \rightarrow X_s \gamma) \times 10^4$	3.55	0.26	0.30	[45]
$R_{\Delta M_{B_s}}$	1.04	0.11	-	[46]
$\frac{\text{BR}(\bar{B}_u \rightarrow \tau \nu)}{\text{BR}(\bar{B}_u \rightarrow \tau \nu)_{SM}}$	1.63	0.54	-	[45]
$\Delta_{0-} \times 10^2$	3.1	2.3	-	[47]
$\frac{\text{BR}(B \rightarrow D \tau \nu)}{\text{BR}(B \rightarrow D e \nu)} \times 10^2$	41.6	12.8	3.5	[48]
R_{l23}	0.999	0.007	-	[49]
$\text{BR}(D_s \rightarrow \tau \nu) \times 10^2$	5.38	0.32	0.2	[45]
$\text{BR}(D_s \rightarrow \mu \nu) \times 10^3$	5.81	0.43	0.2	[45]
$\text{BR}(D \rightarrow \mu \nu) \times 10^4$	3.82	0.33	0.2	[45]
$\Omega_\chi h^2$	0.1196	0.0031	0.012	[50]
m_h [GeV]	125.66	0.41	2.0	[51]
$\text{BR}(\bar{B}_s \rightarrow \mu^+ \mu^-)$	3.2×10^{-9}	1.5×10^{-9}	10%	[52]
	Limit (95% CL)			Ref.
Sparticle masses	As in Table 4 of Ref. [53].			
$m_\chi - \sigma_{\chi N}^{\text{SI}}$	XENON100 2012 limits			[23]

TABLE I. Observables used for the computation of the likelihood function

a multiplication of individual likelihood functions, where for each quantity we use a gaussian function with mean μ and standard deviation $s = \sqrt{\sigma^2 + \tau^2}$, where σ is the experimental uncertainty and τ represents our estimate of the theoretical uncertainty. For upper and lower limits we use a gaussian function to model the drop in the likelihood below or above the experimental bound. The explicit form of the likelihood function is given in ref. [53], including in particular a smearing out of experimental errors and limits to include an appropriate theoretical uncertainty in the observables. We take into consideration all the available particle physics data described in table I, including the Z mass, which is effectively included adding a Jacobian factor¹, electroweak precision measurements [54], B-physics observables [46, 48, 49, 52, 55], the Higgs mass [6, 7], and constraints on the WIMP-nucleon scattering cross-section by XENON-100 [23] and LUX [24]. In addition, we assume a scenario with a single dark matter component that is produced thermally in the early Universe, by including the measured relic density according to the *Planck* results [56]. For the relic density and $\langle \sigma v \rangle$ computation, we take the SE into account by creating a grid of the enhancement in the M_2 - μ plane using the Hryczuk et al. computation method implemented in DarkSE [17, 18]. For the computation of $\langle \sigma v \rangle$ in the present day we implemented a function in DarkSE to extract the enhancement for $v = 10^{-3}$ from the Hryczuk *et al.* computation (we validated the results with the pure-wino case showed in [18]).

¹ The Jacobian factor arise after perform a change of variable $\{y_i, \mu, B\} \rightarrow \{m_i, M_z, \tan \beta\}$ and integrating M_z in the posterior probability density function, as explained in detail in Ref.[31].

Parameters	Range scanned
M_1, M_2, M_3 [GeV]	$(-10^6, 10^6)$
$m_{\tilde{g}}, m_{\tilde{b}}, m_H$ [GeV]	$(10, 10^6)$
A_0^q, A_0^l [GeV]	$(-10^6, 10^6)$
$\tan \beta$	$(2, 60)$
$\text{sgn}(\mu)$	+1

TABLE II. Ranges of model parameters adopted in the scan.

	Gaussian prior	Range scanned	ref.
M_t [GeV]	173.2 ± 0.9	$(167.0, 178.2)$	[51]
$m_b(m_b)^{\overline{MS}}$ [GeV]	4.20 ± 0.07	$(3.92, 4.48)$	[57]
$[\alpha_{em}(M_Z)^{\overline{MS}}]^{-1}$	127.955 ± 0.030	$(127.835, 128.075)$	[57]
$\alpha_s(M_Z)^{\overline{MS}}$	0.1176 ± 0.0020	$(0.1096, 0.1256)$	[58]

TABLE III. Nuisance parameters adopted in the scan.

For the priors of the parameters, we adopted both standard and ‘improved’ log priors (S-log and I-log, respectively), defined in Refs. [8, 9], with ranges described in table II. In the case of the I-log priors, we effectively assume that the parameters are associated with a common scale (motivated by a common underlying supersymmetry breaking mechanism). In the following, we show results for the I-log priors only, but note that those obtained with S-log priors are very similar, since the data, in particular the relic density constraint and the Higgs mass, turns out to be very constraining. For the SM parameters, we used gaussian priors described in table III. For the numerical analysis, we use the SuperBayeS code [59], which uses the nested sampling algorithm implemented in Multinest [60], and integrates SoftSusy [61], SusyBSG [62], SuperIso [63], DarkSusy [64], MicrOMEGAs [65], and DarkSE [17] for the computation of the experimental observable. The full likelihood function is the product of the individual gaussian likelihoods associated to each piece of experimental data. In particular, for Xenon100 we use the likelihood defined in [66]. The LUX limit is applied as a step function only for the 2σ confidence level points. For a more detailed explanation of the Bayesian analysis relevant for the results in this paper, we refer the reader to Ref. [9].

III. RESULTS OF THE SCAN

In Fig. 1, we show two-dimensional contours that represent 68% and 95% credible regions of the most relevant parameters for CTA: the dark matter neutralino mass and annihilation cross-section. The posterior has two peaks in the mass distribution. The largest peak locates around 1 TeV, where the neutralino mostly consists of higgsino. There is a weaker peak around 3 TeV, where it is mostly wino. The wino dark matter features significantly larger annihilation cross-section around $10^{-24} \text{ cm}^3 \text{ s}^{-1}$ due to SE correction. Since the SE is a non-relativistic effect causing the distortion of the

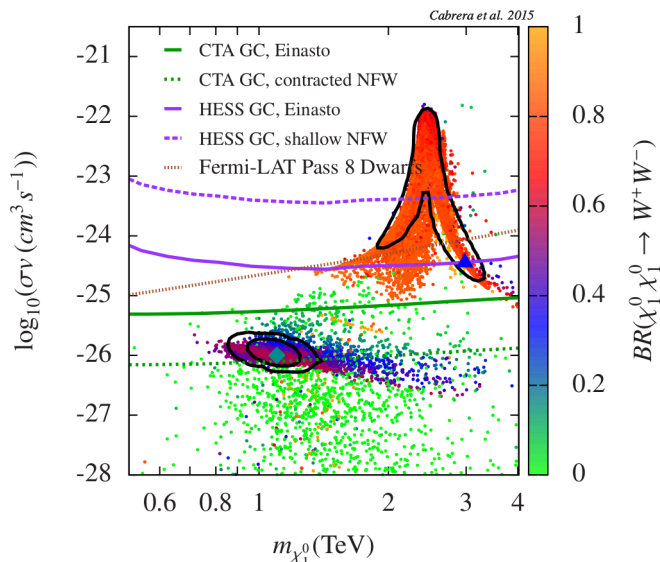


FIG. 1. The contours represent 68% and 95% posterior probability credible regions. Colored points reproduce all the experimental observables within 2σ of confidence level. The cyan diamond represent the pure higgsino case from [67], and the blue triangle the pure wino case from [10, 18]. The color-coding indicates the branching fraction into W^+W^- final states. The green lines show the sensitivity of CTA as derived in Ref. [40] for $b\bar{b}$ final states and 100h observation time (assuming 1% systematics). The purple lines show the HESS Galactic center limits for generic hadronic final states [68], adopting an Einasto (solid), a contracted NFW (dotted), and a shallow NFW (dashed) profiles. The brown dotted line shows the *Fermi*-LAT limit from the analysis of the dwarf spheroidal galaxies [69]. The CTA and *Fermi*-LAT limits correspond to $\chi_1^0\chi_1^0 \rightarrow b\bar{b}$, but limits for W^+W^- final states are very similar.

wave functions, it is more efficient for heavier particles. We note that these two regions correspond to those found in Ref. [9] with a seven-parameter MSSM study. In fact, the most probable regions in the posterior distributions for the mass of the lightest particles (the neutralino) are only mildly changed compared to [9]. This shows the robustness of the procedure against the number of parameters.

Figure 1 also shows, as points, regions in the parameter space that reproduce all experimental observables within 2σ of confidence level. We remind that the posterior probability distribution function (PDF) shows relative probabilities within a model, given the experimental data, under the hypothesis that the model is correct. The 68% and 95% credibility regions show that it is much more likely to find neutralinos with a mass of ~ 1 TeV and ~ 3 TeV, however, these contours not necessarily cover all the regions that respect the experimental observables. The scattered points outside the contours show regions that require more tuning to reproduce the experimental observables and, therefore, their integrated probability is small. These less probable regions, with

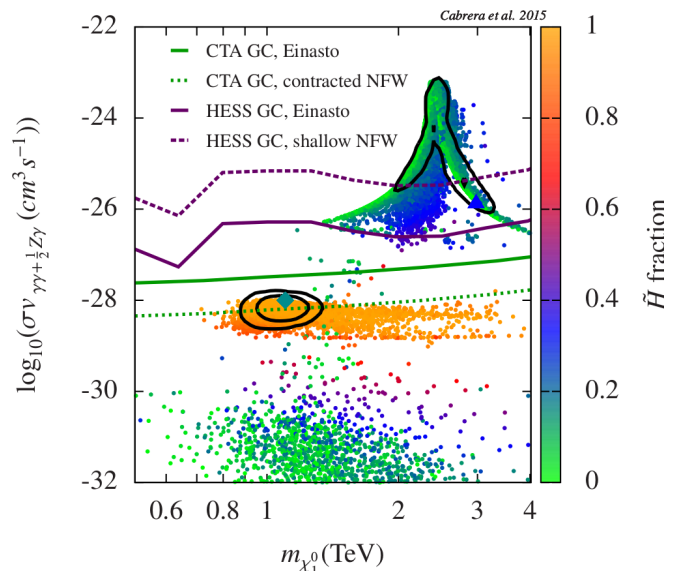


FIG. 2. The same as Fig. 1, but for annihilation into monochromatic photons. The cyan diamond represent the pure higgsino case from [10, 18], and the blue triangle the pure wino case [15]. Colors indicate the higgsino fraction of the lightest neutralino. The green lines show the line sensitivity of CTA as derived from [70], while purple lines are the HESS limits [71], all for the Galactic center.

dark matter between 1 TeV and 3 TeV, correspond to wino-higgsino and wino-bino neutralinos.

An additional region around hundreds GeV, corresponding to bino-like neutralino, is not shown in the figure. Unlike higgsinos and winos, bino neutralinos can not self-annihilate, therefore, a specific mass relation with other mass eigenstate is required to have an efficient enough annihilation to reproduce the correct relic density. For example, a bino quasi-degenerate with the stau, or a bino mass equal to half of the lightest Higgs or pseudo-scalar mass. On the other hand, as we mention above, unless we are in the maximal mixing scenario (which is also subject to certain tuning, see Ref. [72]) the Higgs mass measurement tend to push the spectrum to higher masses. For few hundreds GeV neutralinos, a fine-tuning is necessary to reproduce the Higgs mass and the relic density. Therefore, this region has small statistical weight and is not well explored in our scan. For this reason we show $m_{\chi_1^0}$ larger than 500 GeV in our figures. In any case, few hundreds GeV neutralinos will be potentially tested by the LHC.

The annihilation of wino-like dark matter produces relatively strong line signatures. Given that the total annihilation cross-section is very large, as shown in Fig. 1, the resulting annihilation cross-section into $\gamma\gamma$ or γZ channel is correspondingly large. Figure 2 shows the contours of mass and $\langle\sigma v\rangle_{\gamma\gamma} + \langle\sigma v\rangle_{\gamma Z}/2$, which is the relevant quantity for line searches with Cherenkov telescopes since the energy splitting between these two modes are smaller

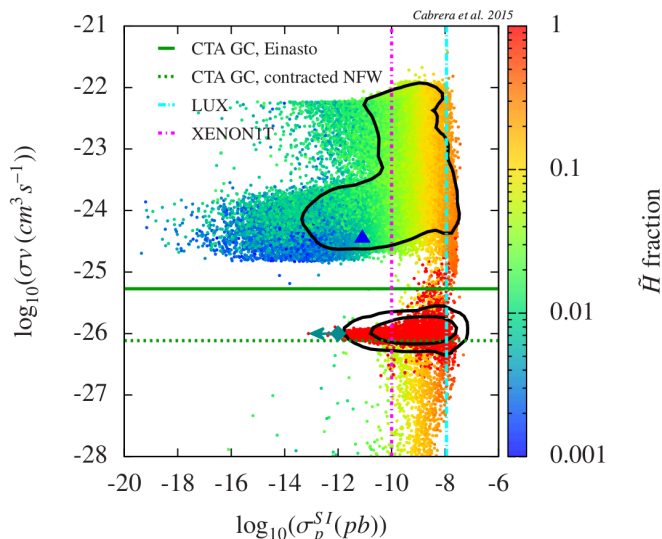


FIG. 3. Similar to Fig. 1, but showing the total annihilation cross-section against the WIMP-proton spin-independent cross-section. The blue triangle and the cyan arrow are the theoretical values of the pure wino and pure higgsino case from Refs. [73, 74]. The arrow indicates that the value of σ_p^{SI} is a theoretical upper limit. The color-coding indicates the higgsino fraction. Green lines show the sensitivity of CTA for Einasto (solid) and contracted NFW (dotted) profiles for the Galactic center [40]. Cyan and pink lines represent LUX limit [24] and XENON-1T sensitivity [32]. Both the limit and sensitivity lines assume $m_{\chi_1^0} = 1$ TeV. CTA sensitivity lines correspond to $\chi_1^0 \chi_1^0 \rightarrow b\bar{b}$.

than their typical energy resolution (e.g., Ref. [10]).

The colored points in Fig. 1 show the branching fraction of the lightest neutralino annihilating into W^+W^- . For the higgsino-like neutralino ($m_{\chi_1^0} \sim 1$ TeV), the annihilation to ZZ becomes very important, while for the wino-like neutralino ($m_{\chi_1^0} \sim 3$ TeV), the annihilation to W^+W^- is the dominant channel. The colored points in Fig. 2 shows the higgsino fraction of the lightest neutralino. Note that points inside the 95% contour are dominantly higgsino-like and wino-like neutralinos. However, by comparing those points with the pure higgsino (cyan diamond) and pure wino (blue triangle) cases, it is clear that the 95% contour encloses points with small mixing that could have different characteristics. In particular, in the wino-like region with $\langle\sigma v\rangle_{\gamma\gamma+\gamma Z/2} > 10^{-27}$ cm³/s and $m_{\chi_1^0} \sim 2.5$ TeV, the co-annihilation with sfermions plays a very important role in setting the correct relic density.

IV. GAMMA-RAY UPPER LIMITS AND PROSPECTS

The Galactic center is one of the most promising places to search for signals from WIMP annihilation, as it is

locally the densest region of dark matter, even though it is often challenging to address astrophysical foregrounds (see, e.g., Ref. [75]). In general, the gamma-ray intensity from neutralino annihilation towards a direction ψ away from the Galactic center is given by

$$I_\gamma(\psi, E_\gamma) = \frac{\langle\sigma v\rangle}{8\pi m_{\chi_1^0}^2} \frac{dN_{\gamma,\text{ann}}}{dE_\gamma} J(\psi), \quad (3)$$

$$J(\psi) = \int_0^{l_{\text{max}}} dl \rho_{\chi_1^0}^2(r[l, \psi]),$$

where $dN_{\gamma,\text{ann}}/dE_\gamma$ represents the annihilation spectrum, $r(l, \psi)^2 = r_0^2 + l^2 - 2r_0l \cos \psi$, $r_0 = 8.5$ kpc is the Galactocentric radius of the solar system, and l_{max} corresponds to the virial radius of the Milky Way. The dark matter density profile in the Galactic halo $\rho_{\chi_1^0}$ is widely assumed to be given by phenomenological fits to results of dark-matter-only N-body simulations, such as the Navarro-Frenk-White (NFW) [76] or Einasto [77, 78] functions. We note, however, that these profiles are observationally confirmed only at relatively large radii, and far less constrained in the inner regions [79], where the strongest annihilation signals are expected. We will comment again on this point below.

a. Current Status. Figures 1 and 2 show the predicted annihilation cross-section into continuum photons (dominated by W^+W^- , ZZ and $\bar{q}q$ final states) and gamma-ray lines, respectively, compared to different experimental limits and reaches. Our fiducial density profile is given by an Einasto profile (with parameters $\alpha = 0.17$, $\rho_\odot = 0.4$ GeV/cm³ and $r_s = 20$ kpc). The current upper limits on the Galactic center from HESS searches for gamma rays from $b\bar{b}$ final states (Fig. 1) [68] [71] and for gamma-ray lines (Fig. 2) [71] are already very tight. We find that the wino dark matter region around 3 TeV is almost completely excluded by the HESS upper limits. This is in agreement with the findings of Refs. [10–12], but interpolating in the σv enhancement from a $M_2 - -\mu$ grid instead of extrapolated from existing pure wino calculations as is in Ref. [34].

We note, however, that upper limits are still subject to uncertainties mainly related to the density profile [10]. While state-of-the-art N-body simulations prefer either NFW or Einasto profiles, baryonic effects can potentially modify the density profiles significantly. For example, baryonic adiabatic contraction can compress the dark matter profiles, while supernova feedback can cause the profiles to be shallower (see, e.g., Refs. [80–83]). To illustrate this point, we show in Figs. 1 and 2 how the HESS limits weaken when a shallower dark matter profile is adopted. To this end, we use a generalized NFW profile with an inner slope of $\gamma = 0.7$ (and $r_s = 20$ kpc, $\rho_\odot = 0.4$ GeV/cm³), which is still in agreement with kinematic and microlensing observations [79]. In this case, the limits indeed are weakened and part of the wino best-fit region is still allowed. A similar effect will occur for cored profiles.

In Fig. 1, we also show the *Fermi*-LAT limits from the observation of dwarf spheroidal galaxies from Ref. [69], which already include the uncertainties in the dark matter profile and can be hence considered robust (i.e., they represent the upper end of the uncertainty band). They exclude most of the wino parameter space.

b. Prospects for CTA. Current constraints leave the 1-TeV higgsino dark matter as most interesting dark matter candidate in the MSSM-9. The CTA sensitivities for both the total annihilation cross section [40] and for the gamma-ray lines [70] are shown in Figs. 1 and 2, respectively. These figures show that, for standard Einasto profiles, it will be challenging for CTA to reach the 1-TeV higgsino parameter space, unless background systematics are under control at the sub-percent level [40]. However, as explained above, baryonic effects could potentially increase the chances for a CTA discovery of higgsino dark matter as baryons can drag dark matter towards the Galactic center during their cooling, leading to a more cuspy profile [80]. To illustrate this effect, we additionally show in Fig. 1 the reach of CTA when a slightly contracted NFW profile, with an inner slope of $\gamma = 1.3$ (and otherwise parameters as above), is adopted. In this case, CTA has the potential to rule out (or discover) a large part of the best-fit higgsino dark matter region. Our results are less stringent than the results found in Ref. [34], since our estimates for the CTA sensitivity also include an estimated 1% systematic uncertainty. Note also that a more accurate treatment of the cosmic ray background in Ref. [41] leads, for dark matter masses above 1 TeV, to slightly less stringent projected limits than what we show here, within a factor of two.

c. Direct Detection. Fig. 3 shows the most probable regions plotted for the annihilation cross-section and the spin-independent scattering cross-section σ_p^{SI} at tree level. To give a reference of the size of σ_p^{SI} for pure cases, we also show higgsino neutralino (cyan diamond) and wino neutralino (blue triangle) one-loop computation performed by [73, 74].² In the pure higgsino case, the perturbative QCD and hadronic input 1σ -uncertainties allow only to set a maximum value for σ_p^{SI} , which is represented in the figure by an arrow.³ Hence, the mixing of the neutralino has a crucial role for the computation of σ_p^{SI} . The colored points in Fig. 3 represent the higgsino composition of the lightest neutralino, and show

how the value of σ_p^{SI} decreases with the higgsino fraction in the wino-like region. We remind the reader that this computation was performed at tree level in our scan. However, almost pure wino points appear in the region where σ^{SI} is smaller than $\sim 10^{-11}$ pb and σv larger than 10^{-25} cm³ s⁻¹ in Fig. 3. Comparing these σ^{SI} values with the one of the pure wino case (blue triangle), it is clear that the one-loop contribution is the dominant one. Therefore, we would expect that after including higher order corrections those points will get σ^{SI} values of $\sim 10^{-11}$ pb.

Figure 3 also shows the sensitivities of XENON-1T [32] and CTA [40] (both for $m_{\chi_1^0} = 1$ TeV), showing that both direct and indirect searches are very important for the potential discovery of TeV dark matter, that is, at the moment, the most probable solution in the context of MSSM-9. Note also that the region around the almost-pure and pure wino and higgsino neutralinos will be probed by CTA only.

V. CONCLUSIONS

We studied the prospects for indirect and direct dark matter searches in context of the MSSM-9 by means of a Bayesian Monte Carlo scan. We find as the two most likely regions the 1-TeV higgsinos and 3-TeV winos dark matter. Current limits from dwarf spheroidal observations as well as observations of the Galactic center with *Fermi*-LAT and HESS exclude almost all the models with wino-like dark matter, even for flattened profiles of the dark matter halo. However, models with 1-TeV higgsino-like dark matter remain unconstrained. We find that for regular dark matter profiles, it will be challenging for CTA to probe the higgsino dark matter parameter space, both for continuum and gamma-ray line searches. However, a mildly contracted profile would improve the prospects significantly, and make most of the higgsino dark matter parameter space testable in the upcoming years, providing complementary constraints to future direct detection experiments like XENON-1T.

ACKNOWLEDGMENTS

We thank Andrzej Hryczuk for providing us numerical routines and giving useful advices for the calculation of the Sommerfeld enhancement, Paolo Panci and Mattia Fornasa for useful discussions. Furthermore, we thank the anonymous referee for pointing out an error in the production of $\bar{f}f$ final states in the first version of this manuscript. This research was supported by the Munich Institute for Astro- and Particle Physics (MIAPP) of the DFG cluster of excellence ‘‘Origin and Structure of the Universe’’. Furthermore, the work was supported by NWO through one Veni and two Vidi grants (SA, CW and FZ), by Fundaao de Amparo a Pesquisa do Estado de Sao Paulo (MECC) and by the Spanish MICINN

² The tree level scattering of the neutralino with the nucleon, through the Higgs boson, requires a neutralino with non-negligible higgsino-bino or higgsino-wino mixing. The other possibility is the scattering via squarks, in that case squarks should be light enough to give a sizable contribution.

³ For the computation of σ^{SI} we have used the s-quarks nucleon form factor derived from measurements of the pion-nucleon sigma term [84]. On the other hand, refs. [73, 74] use the lattice calculation value. Using the lattice value the tree level cross section drops by a factor of 4 ref [85].

- [1] G. Jungman, M. Kamionkowski, and K. Griest, *Phys.Rept.* **267**, 195 (1996), arXiv:hep-ph/9506380 [hep-ph].
- [2] G. Bertone, D. Hooper, and J. Silk, *Phys.Rept.* **405**, 279 (2005), arXiv:hep-ph/0404175 [hep-ph].
- [3] T. Bringmann and C. Weniger, *Phys.Dark Univ.* **1**, 194 (2012), arXiv:1208.5481 [hep-ph].
- [4] G. Steigman, B. Dasgupta, and J. F. Beacom, *Phys.Rev.* **D86**, 023506 (2012), arXiv:1204.3622 [hep-ph].
- [5] M. Ackermann *et al.* (Fermi-LAT Collaboration), *Phys.Rev.* **D89**, 042001 (2014), arXiv:1310.0828 [astro-ph.HE].
- [6] G. Aad *et al.* (ATLAS Collaboration), *Phys.Lett.* **B716**, 1 (2012), arXiv:1207.7214 [hep-ex].
- [7] S. Chatrchyan *et al.* (CMS Collaboration), *Phys.Lett.* **B716**, 30 (2012), arXiv:1207.7235 [hep-ex].
- [8] M. E. Cabrera, J. A. Casas, and R. R. de Austri, *JHEP* **1307**, 182 (2013), arXiv:1212.4821 [hep-ph].
- [9] M. E. Cabrera, A. Casas, R. R. de Austri, and G. Bertone, *JHEP* **1412**, 114 (2014), arXiv:1311.7152 [hep-ph].
- [10] T. Cohen, M. Lisanti, A. Pierce, and T. R. Slatyer, *JCAP* **1310**, 061 (2013), arXiv:1307.4082.
- [11] J. Fan and M. Reece, *JHEP* **1310**, 124 (2013), arXiv:1307.4400 [hep-ph].
- [12] A. Hryczuk, I. Cholis, R. Iengo, M. Tavakoli, and P. Ullio, *JCAP* **1407**, 031 (2014), arXiv:1401.6212 [astro-ph.HE].
- [13] J. Hisano, S. Matsumoto, and M. M. Nojiri, *Phys.Rev.Lett.* **92**, 031303 (2004), arXiv:hep-ph/0307216 [hep-ph].
- [14] J. Hisano, S. Matsumoto, M. M. Nojiri, and O. Saito, *Phys.Rev.* **D71**, 063528 (2005), arXiv:hep-ph/0412403 [hep-ph].
- [15] M. Cirelli, A. Strumia, and M. Tamburini, *Nucl.Phys.* **B787**, 152 (2007), arXiv:0706.4071 [hep-ph].
- [16] N. Arkani-Hamed, D. P. Finkbeiner, T. R. Slatyer, and N. Weiner, *Phys.Rev.* **D79**, 015014 (2009), arXiv:0810.0713 [hep-ph].
- [17] A. Hryczuk, R. Iengo, and P. Ullio, *JHEP* **1103**, 069 (2011), arXiv:1010.2172 [hep-ph].
- [18] A. Hryczuk and R. Iengo, *JHEP* **1201**, 163 (2012), arXiv:1111.2916 [hep-ph].
- [19] M. Baumgart, I. Z. Rothstein, and V. Vaidya, (2014), arXiv:1409.4415 [hep-ph].
- [20] M. Bauer, T. Cohen, R. J. Hill, and M. P. Solon, *JHEP* **1501**, 099 (2015), arXiv:1409.7392 [hep-ph].
- [21] G. Ovanessian, T. R. Slatyer, and I. W. Stewart, (2014), arXiv:1409.8294 [hep-ph].
- [22] M. Baumgart, I. Z. Rothstein, and V. Vaidya, (2014), arXiv:1412.8698 [hep-ph].
- [23] E. Aprile *et al.* (XENON100 Collaboration), *Phys.Rev.Lett.* **109**, 181301 (2012), arXiv:1207.5988 [astro-ph.CO].
- [24] D. Akerib *et al.* (LUX Collaboration), *Phys.Rev.Lett.* **112**, 091303 (2014), arXiv:1310.8214 [astro-ph.CO].
- [25] H. Silverwood, P. Scott, M. Danninger, C. Savage, J. Edsj, *et al.*, *JCAP* **1303**, 027 (2013), arXiv:1210.0844 [hep-ph].
- [26] S. Akula, P. Nath, and G. Peim, *Phys.Lett.* **B717**, 188 (2012), arXiv:1207.1839 [hep-ph].
- [27] O. Buchmueller, R. Cavanaugh, M. Citron, A. De Roeck, M. Dolan, *et al.*, *Eur.Phys.J.* **C72**, 2243 (2012), arXiv:1207.7315.
- [28] A. Fowlie, M. Kazana, K. Kowalska, S. Munir, L. Roszkowski, *et al.*, *Phys.Rev.* **D86**, 075010 (2012), arXiv:1206.0264 [hep-ph].
- [29] O. Buchmueller, R. Cavanaugh, A. De Roeck, M. Dolan, J. Ellis, *et al.*, *Eur.Phys.J.* **C74**, 2922 (2014), arXiv:1312.5250 [hep-ph].
- [30] L. Roszkowski, E. M. Sessolo, and A. J. Williams, *JHEP* **1408**, 067 (2014), arXiv:1405.4289 [hep-ph].
- [31] M. Cabrera, J. Casas, and R. Ruiz de Austri, *JHEP* **0903**, 075 (2009), arXiv:0812.0536 [hep-ph].
- [32] E. Aprile (XENON1T collaboration), *Springer Proc.Phys.* **C12-02-22**, 93 (2013), arXiv:1206.6288 [astro-ph.IM].
- [33] M. Actis, G. Agnetta, F. Aharonian, A. Akhperjanian, J. Aleksić, E. Aliu, D. Allan, I. Alekotte, F. Antico, L. A. Antonelli, and *et al.*, *Experimental Astronomy* **32**, 193 (2011), arXiv:1008.3703 [astro-ph.IM].
- [34] L. Roszkowski, E. M. Sessolo, and A. J. Williams, *JHEP* **1502**, 014 (2015), arXiv:1411.5214 [hep-ph].
- [35] A. Abramowski *et al.* (H.E.S.S. Collaboration), *Phys.Rev.Lett.* **110**, 041301 (2013), arXiv:1301.1173 [astro-ph.HE].
- [36] J. Hisano, S. Matsumoto, and M. M. Nojiri, *Phys.Rev.* **D67**, 075014 (2003), arXiv:hep-ph/0212022 [hep-ph].
- [37] M. Doro *et al.* (CTA collaboration), *Astropart.Phys.* **43**, 189 (2013), arXiv:1208.5356 [astro-ph.IM].
- [38] M. Wood, J. Buckley, S. Digel, S. Funk, D. Nieto, *et al.*, (2013), arXiv:1305.0302 [astro-ph.HE].
- [39] M. Pierre, J. M. Siegal-Gaskins, and P. Scott, *JCAP* **1406**, 024 (2014), arXiv:1401.7330 [astro-ph.HE].
- [40] H. Silverwood, C. Weniger, P. Scott, and G. Bertone, (2014), arXiv:1408.4131 [astro-ph.HE].
- [41] V. Lefranc, E. Moulin, P. Panci, and J. Silk, (2015), arXiv:1502.05064 [astro-ph.HE].
- [42] M. S. Carena, J. Espinosa, M. Quiros, and C. Wagner, *Phys.Lett.* **B355**, 209 (1995), arXiv:hep-ph/9504316 [hep-ph].
- [43] H. E. Haber, R. Hempfling, and A. H. Hoang, *Z.Phys.* **C75**, 539 (1997), arXiv:hep-ph/9609331 [hep-ph].
- [44] <http://lepewwg.web.cern.ch/LEPEWWG>.
- [45] Y. Amhis *et al.* (Heavy Flavor Averaging Group), (2012), arXiv:1207.1158 [hep-ex].
- [46] R. Aaij *et al.* (LHCb Collaboration), *Phys.Lett.* **B709**, 177 (2012), arXiv:1112.4311 [hep-ex].
- [47] B. Aubert *et al.* (BABAR), (2008), arXiv:0808.1915 [hep-ex].
- [48] B. Aubert *et al.* (BaBar Collaboration), *Phys.Rev.Lett.* **100**, 021801 (2008), arXiv:0709.1698 [hep-ex].
- [49] M. Antonelli *et al.* (FlaviaNet Working Group on Kaon Decays), (2008), arXiv:0801.1817 [hep-ph].
- [50] P. Ade *et al.* (Planck), *Astron.Astrophys.* **571**, A16 (2014), arXiv:1303.5076 [astro-ph.CO].

- [51] J. D. Etienne Auge and J. T. T. Van, (2013).
- [52] R. Aaij *et al.* (LHCb Collaboration), *Phys.Rev.Lett.* **110**, 021801 (2013), arXiv:1211.2674 [hep-ex].
- [53] R. R. de Austri, R. Trotta, and L. Roszkowski, *JHEP* **0605**, 002 (2006), arXiv:hep-ph/0602028 [hep-ph].
- [54] “The LEP Electroweak Working Group,” <http://lepewwg.web.cern.ch/LEPEWWG>.
- [55] Y. Amhis *et al.* (Heavy Flavor Averaging Group), (2012), arXiv:1207.1158 [hep-ex].
- [56] P. Ade *et al.* (Planck), *Astron.Astrophys.* **571**, A16 (2014), arXiv:1303.5076 [astro-ph.CO].
- [57] W. Yao *et al.* (Particle Data Group), *J.Phys.* **G33**, 1 (2006).
- [58] K. Hagiwara, A. Martin, D. Nomura, and T. Teubner, *Phys.Lett.* **B649**, 173 (2007), arXiv:hep-ph/0611102 [hep-ph].
- [59] C. Strege, G. Bertone, G. Besjes, S. Caron, R. Ruiz de Austri, *et al.*, *JHEP* **1409**, 081 (2014), arXiv:1405.0622 [hep-ph].
- [60] F. Feroz, M. Hobson, and M. Bridges, *Mon.Not.Roy.Astron.Soc.* **398**, 1601 (2009), arXiv:0809.3437 [astro-ph].
- [61] B. Allanach, *Comput.Phys.Commun.* **143**, 305 (2002), arXiv:hep-ph/0104145 [hep-ph].
- [62] G. Degrassi, P. Gambino, and P. Slavich, *Comput.Phys.Commun.* **179**, 759 (2008), arXiv:0712.3265 [hep-ph].
- [63] F. Mahmoudi, *Comput.Phys.Commun.* **180**, 1579 (2009), arXiv:0808.3144 [hep-ph].
- [64] P. Gondolo, J. Edsjo, P. Ullio, L. Bergstrom, M. Schelke, *et al.*, *JCAP* **0407**, 008 (2004), arXiv:astro-ph/0406204 [astro-ph].
- [65] G. Belanger, F. Boudjema, A. Pukhov, and A. Semenov, *Comput.Phys.Commun.* **149**, 103 (2002), arXiv:hep-ph/0112278 [hep-ph].
- [66] G. Bertone, D. G. Cerdeno, M. Fornasa, R. Ruiz de Austri, C. Strege, *et al.*, *JCAP* **1201**, 015 (2012), arXiv:1107.1715 [hep-ph].
- [67] S. Profumo, *Phys.Rev.* **D72**, 103521 (2005), arXiv:astro-ph/0508628 [astro-ph].
- [68] A. Abramowski *et al.* (HESS Collaboration), *Phys.Rev.Lett.* **106**, 161301 (2011), arXiv:1103.3266 [astro-ph.HE].
- [69] M. Ackermann *et al.* (Fermi-LAT), (2015), arXiv:1503.02641 [astro-ph.HE].
- [70] L. Bergstrom, G. Bertone, J. Conrad, C. Farnier, and C. Weniger, *JCAP* **1211**, 025 (2012), arXiv:1207.6773 [hep-ph].
- [71] A. Abramowski *et al.* (H.E.S.S. Collaboration), *Phys.Rev.Lett.* **110**, 041301 (2013), arXiv:1301.1173 [astro-ph.HE].
- [72] J. A. Casas, J. M. Moreno, S. Robles, K. Rolbiecki, and B. Zaldivar, (2014), arXiv:1407.6966 [hep-ph].
- [73] R. J. Hill and M. P. Solon, *Phys.Rev.Lett.* **112**, 211602 (2014), arXiv:1309.4092 [hep-ph].
- [74] R. J. Hill and M. P. Solon, *Phys.Rev.* **D91**, 043505 (2015), arXiv:1409.8290 [hep-ph].
- [75] F. Calore, I. Cholis, and C. Weniger, ArXiv e-prints (2014), arXiv:1409.0042.
- [76] J. F. Navarro, C. S. Frenk, and S. D. White, *Astrophys.J.* **490**, 493 (1997), arXiv:astro-ph/9611107 [astro-ph].
- [77] A. W. Graham, D. Merritt, B. Moore, J. Diemand, and B. Terzic, *Astron.J.* **132**, 2685 (2006), arXiv:astro-ph/0509417 [astro-ph].
- [78] J. F. Navarro, A. Ludlow, V. Springel, J. Wang, M. Vogelsberger, *et al.*, *Mon.Not.Roy.Astron.Soc.* **402**, 21 (2010), arXiv:0810.1522 [astro-ph].
- [79] F. Iocco, M. Pato, G. Bertone, and P. Jetzer, *JCAP* **1111**, 029 (2011), arXiv:1107.5810 [astro-ph.GA].
- [80] F. Prada, A. Klypin, J. Flix, M. Martínez, and E. Simonneau, *Physical Review Letters* **93**, 241301 (2004), astro-ph/0401512.
- [81] A. Pontzen and F. Governato, *MNRAS* **421**, 3464 (2012), arXiv:1106.0499 [astro-ph.CO].
- [82] G. A. Gómez-Vargas, M. A. Sánchez-Conde, J.-H. Huh, M. Peiró, F. Prada, A. Morselli, A. Klypin, D. G. Cerdeño, Y. Mambrini, and C. Muñoz, *JCAP* **10**, 029 (2013), arXiv:1308.3515 [astro-ph.HE].
- [83] A. Del Popolo and F. Pace, (2015), arXiv:1502.01947.
- [84] J. R. Ellis, K. A. Olive, and C. Savage, *Phys.Rev.* **D77**, 065026 (2008), arXiv:0801.3656 [hep-ph].
- [85] J. L. Feng, K. T. Matchev, and D. Sanford, *Phys.Rev.* **D85**, 075007 (2012), arXiv:1112.3021 [hep-ph].